VISIBLE AND NIR BRDF MEASUREMENTS OF LUNAR SOIL SIMULANT. K. Gunderson[1], J. Whitby[1], and N. Thomas[1], [1]Physikalisches Institut, University of Bern, Sidlerstrasse 5, 3012 Bern, Switzerland; kurt.gunderson@phim.unibe.ch.

Introduction: Bidirectional reflectance distribution functions (BRDFs) characterize the outgoing intensity of light from illuminated surfaces according to the illumination and observation geometries of those surfaces. Complete BRDF measurements for extraterrestrial objects over a full 2π steradians are rarely possible because the solar position at the time of observation tends to dictate the system geometry irregardless of whether the observation point is on Earth or a spacecraft. Additionally, zero phase angle observations are rarely possible, especially for inner solar system objects. Consequently, surface reflectances for many geometries must be inferred from models [*e.g.* 1–4] that have been fit to the available data.

A practical example is the need for reflectances of surfaces that are being measured with laser altimeters. Since such instruments [*e.g.* 5–9] operate at effectively zero phase angle, reflectances of the underlying surfaces must be known at zero phase angle in order to determine link budgets and define specifications for the instruments. Zero phase NIR reflectance of Mercury is of particular importance to [8, 9], but no such data are available. However, BRDF models that have been fitted to a set of reflectance measurements [10, 11] can be extrapolated to zero phase angle in order to estimate typical normal albedos [9].

Because the validity of such extrapolations is questionable, and at risk of introducing further questions of the similarity of the Moon and Mercury, we have performed BRDF measurements of lunar soil simulant JSC-1 [12] and discuss results in the context of Hermean reflectance.

Apparatus: The experiment used to perform the measurements was first described in [13]. It uses a quartz-tungsten halogen lamp, collimating optics, and flat mirrors to direct a chopped beam of filtered light onto a sample with a ~1.5° full cone beam divergence angle. The illumination angle is free to vary from θ_i=±90° zenith angle. A Si photodiode can be positioned at θ_e =±90° zenith angle and φ=±180° azimuth angle to measure the scattered light brightness from within the entire illuminated footprint. Vignetting of the beam by receiver hardware restricts the phase angle to be >2.4°. A lock-in amplifier increases sensitivity to analog diode outputs, and is readout digitally via an RS-232 serial stream.

Samples: Test samples included basaltic JSC-1 lunar soil simulant [12] and a PTFE (polytetrafluoroethene) reflectance standard, which has a hemispheric albedo of $A_{H,PTFE}$≈98% from 400–1500 nm according to vendor documentation. The lunar simulant sample was prepared by first leveling it and then sprinkling 1–2 mm of loose material over a packed surface. Data were taken using a visible light filter with central wavelength λ_V=561 nm (green) and $\delta\lambda_V$=69 nm FWHM, and a near infrared filter with a transmission window extending from 800 nm beyond the Si cutoff around 1100 nm such that λ_{NIR}≈950 nm and $\delta\lambda_{NIR}$≈300 nm.

Data and analysis: Four angular scans were made using each filter. One scan measured the photodiode output voltage due to scattered light off of the reflectance standard (V_{PTFE}) under normal illumination (θ_i=0°) and from θ_e =0 to 90° in 1° steps. Another scan repeated the measurement for the soil simulant. Two other scans measured V_S of the soil simulant at near-zero phase angles of –3° and 4° from θ_e =–65 to 65° in 1° steps. Under the assumption that the sample would scatter isotropically at fixed θ_i and θ_e, φ was kept at 0° such that the illumination and emission axes were always coplanar. Since the detector receives scattered light from within the entire footprint,

$$r_\lambda = \frac{C_\lambda V(\lambda,\theta_e)}{\cos\theta_e}\ \mathrm{sr}^{-1},$$

where r_λ is the reflectance, and C_λ is a normalization coefficient determined using reflectance standard data according to:

$$C_\lambda = \frac{A_{H,PTFE}}{2\pi}\left[\int_o^{\pi/2} V_{PTFE}(\lambda,\theta_e)\sin\theta_e d\theta_e\right]^{-1}\ \mathrm{sr}^{-1}\ \mathrm{V}^{-1},$$

which presumes azimuthally isotropic emission and vendor-provided $A_{H,PTFE}$. The hemispheric and normal albedos (A_H and A_N, respectively) then can be found according to:

$$A_H = 2\pi C_\lambda \int_0^{\pi/2} V_\lambda(\theta_e)\sin\theta_e d\theta_e$$

$$A_N = \pi C_\lambda V_\lambda(\theta_e = \theta_i).$$

Discussion: Figure 1 shows plots of normalized visible and NIR radiance as functions of phase angle (ϕ) at θ_i=0° for the reflectance standard and lunar soil simulant. Radiance curves have been extended with spline extrapolations to zero phase angle, and the soil simulant data have been multiplied by 5 for clarity. A horizontal line represents the radiance of a perfect

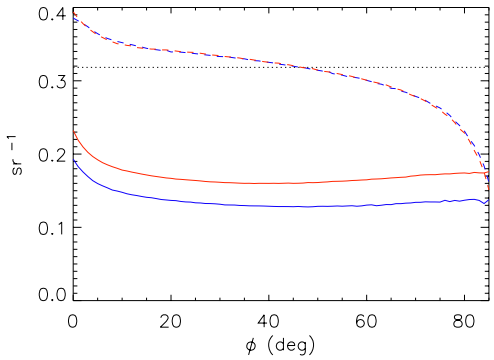

Figure 1. BRDF versus phase angle in the visible and NIR (*blue, red*) for the PTFE reflectance standard and lunar soil simulant (×5) (*dashed, solid*). A BRDF for a perfect Lambert surface is overplotted (*dotted*).

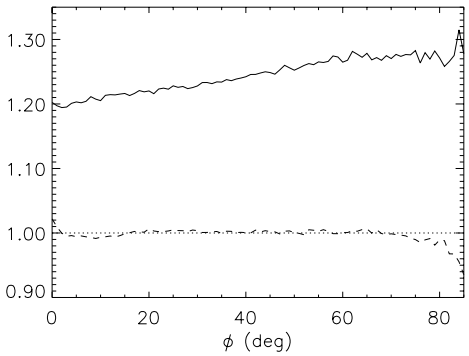

Figure 2. Ratio of NIR BRDF to visible BRDF for soil simulant (solid) and the reflectance standard (dashed). The ratio for a perfect lambert surface is overplotted.

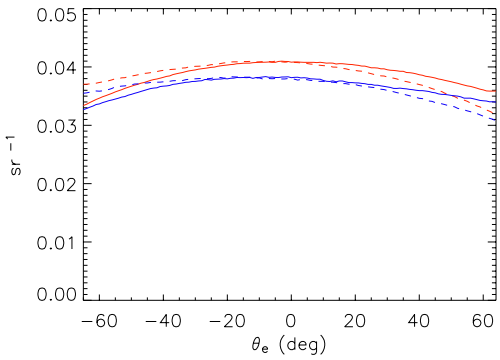

Figure 3. BRDF of lunar soil simulant for θ_i-θ_e=–3 and 4° (*solid, dashed*) and at visible and NIR wavlengths (*blue, red*).

Lambert surface for reference. Both the reflectance standard and the soil simulant data show cusp-like rises towards zero phase angle. However, the reflectance standard cusp is a result of specular reflection off of a smooth surface and the soil simulant cusp is an opposition surge.

Figure 2 shows the ratio of r_{NIR}/r_V for both the soil simulant and reflectance standard. Again, the ratio for a perfect Lambert surface has been overplotted. These data demonstrate that the soil reflectance is higher in the NIR than in the visible, but not by as much as was observed by [14, 15] for Mercury. The plot also reveals a dependency of spectral slope on θ_e, but the sensitivity is less than that reported by [14].

Figure 3 shows near-zero phase angle BRDFs for lunar soil simulant over a range of incidence/emission angles. This plot is of particular relevance to laser altimeter performance, which illuminate/observe potentially sloped planetary surfaces at zero phase angle and possibly along off-nadir optical axes. The asymmetry around θ_e=0° is attributable to the off-zero phase angle, suggesting that the true zero phase angle at a given wavelength lies between the –3 and 4° curves. The ~15% effect observed in these data is much larger than the ~1% effect predicted by the models of [10, 11].

Performing the albedo integrals for these data results in A_H of 0.083 and 0.104 in the visible and NIR, respectively, and A_N of 0.121 and 0.146, ±0.005. The NIR albedo is lower than predicted by BRDF model [10, 11] and spectral slope [14, 15] extrapolation. These data, coupled with discrepancies in near-zero phase data, suggest that either the basaltic JSC-1 lunar soil simulant is not a robust representative of typical Hermean regolith, or the BRDF models do not support arbitrary extrapolations. A lighter, anorthositic sample is being sought for additional testing.

References: [1] B. Hapke (1981) *JGR*, **86**, 3039–3054. [2] B. Hapke (1984) *Icarus* **59**, 41–59. [3] B. Hapke (1986) *Icarus*, **67**, 264–280. [4] B. Hapke (2002) *Icarus*, **157**, 523–534. [5] M. T. Zuber *et al.* (1992) *JGR*, **97**, 7781–7797. [6] P. L. Rustan (1995) *Proc. SPIE*, **2317**, 217–225. [7] T. D. Cole *et al.* (1995) *Proc. SPIE*, **2581**, 2–26. [8] R. E. Gold *et al.* (2001) *P&SS*, **49**, 1467–1479. [9] K. Gunderson *et al.* (2005) *Proc. SPIE*, **5660**, in press. [10] A. Mallama, D. Wang, and R. A. Howard (2002) *Icarus*, **155**, 253–264. [11] J. Warell (2004) *Icarus*, **167**, 271–286. [12] D. S. McKay, *et al.* (1993) *LPS XXIV*, 963–964. [13] K. Gunderson, J. Whitby, and N. Thomas (2004) *LPS XXXV*, Abstract #1662. [14] J. Warell (2002), *Icarus*, **156**, 303-317. [15] A. L. Sprague, *et al.* (2004) *LPS XXXV*, Abstract #1630. [16] J. Warell, *et al.* (2004) *LPS XXXV*, Abstract #1624.

Acknowledgements: The authors wish to thank T. Hosch and J. Schmoegner for their calibration and development work of the measurement apparatus.